HHS Public Access

Author manuscript

Acta Biomater. Author manuscript; available in PMC 2022 September 08.

Published in final edited form as:

Acta Biomater. 2022 August ; 148: 323–335. doi:10.1016/j.actbio.2022.05.051.

Mesh Deformation: a mechanism underlying polypropylene prolapse mesh complications *in vivo*

Katrina M. Knight, PhD[1,2], **Gabrielle E. King, MS**[2], **Stacy L. Palcsey, BS**[2], **Amanda Suda, MS**[3], **Rui Liang, MD**[2,4], **Pamela A. Moalli, MD PhD**[1,4,5]

[(1)]Department of Bioengineering, University of Pittsburgh, Pittsburgh, PA

[(2)]Magee-Womens Research Institute, Pittsburgh, PA

[(3)]School of Medicine, University of Pittsburgh, Pittsburgh, PA

[(4)]Department of Obstetrics, Gynecology and Reproductive Sciences, University of Pittsburgh, Pittsburgh, PA

[(5)]Division of Urogynecology and Reconstructive Pelvic Surgery, Magee-Womens Hospital of the University of Pittsburgh, Pittsburgh, PA

Abstract

Polypropylene meshes used in pelvic organ prolapse (POP) repair are hampered by complications. Most POP meshes are highly unstable after tensioning *ex vivo*, as evidenced by marked deformations (pore collapse and wrinkling) that result in altered structural properties and material burden. By intentionally introducing collapsed pores and wrinkles into a mesh that normally has open pores and remains relatively flat after implantation, we reproduce mesh complications *in vivo*. To do this, meshes were implanted onto the vagina of rhesus macaques in nondeformed (flat) vs deformed (pore collapse +/− wrinkles) configurations and placed on tension. Twelve weeks later, animals with deformed meshes had two complications, 1) mesh exposure through the vaginal epithelium, and 2) myofibroblast proliferation with fibrosis – a mechanism of pain. The overarching response to deformed mesh was vaginal thinning associated with accelerated apoptosis, reduced collagen content, increased proteolysis, deterioration of mechanical integrity, and loss of contractile function consistent with stress shielding – a precursor to mesh exposure. Regional differences were observed, however, with some areas demonstrating myofibroblast

Corresponding Author: Katrina Knight, Magee-Womens Research Institute, 204 Craft Avenue, Pittsburgh, PA 15213, kmk144@pitt.edu, Phone Number: (412) 641-4041, Fax Number: (412) 641-3580.

Declaration of interests

The authors declare that they have no known competing financial interests or personal relationships that could have appeared to influence the work reported in this paper.

We would like to draw the attention of the Editor to the following facts which may be considered as potential declaration of interests: Pamela A. Moalli reports equipment, drugs, or supplies was provided by Coloplast Corp. Katrina M. Knight reports financial support was provided by Magee-Womens Research Institute & Foundation. Pamela A. Moalli reports a relationship with Hologic Inc that includes: board membership. However, there has been no significant financial support for this work that could have influenced its outcome.

proliferation and matrix deposition. Variable mechanical cues imposed by deformed meshes likely induce these two disparate responses. Utilizing meshes associated with uniform stresses on the vagina by remaining flat with open pores after tensioning is critical to improving outcomes.

Graphical Abstract

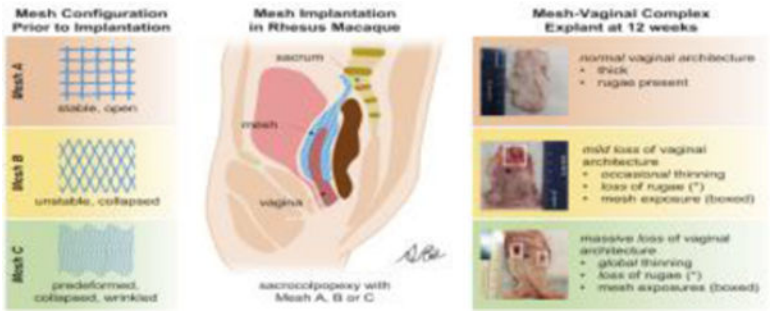

Keywords

synthetic mesh complications; vagina; biomechanical properties; extracellular matrix; stress shielding

1. Introduction

Pelvic organ prolapse (POP), defined as the unnatural descent of the pelvic organs (bladder, rectum, uterus, urethra) into the vagina, is a life-altering condition that primarily impacts aging parous women. Nearly half of all women over the age of 50 experience symptoms of POP, and by the age of 80, approximately 12.6% of women will undergo a surgical repair [1, 2]. Surgeries that utilize the patient's own tissues are associated with high failure rates, up to 70% at 5 years [3, 4]. Therefore, biomaterials like polypropylene meshes are used to augment POP repairs which can be implanted via a transabdominal (sacrocolpopexy) or transvaginal (mesh kits) approach. Transvaginally implanted meshes have been hampered by particularly high complication rates (~20%) [5], leading the FDA to halt the distribution of these products. Complications of meshes implanted via an abdominal approach occur at a lower but still concerning rate (6–10%) that increase over time [6–9]. Pain and exposure of mesh fibers through the vaginal epithelium after vaginal thinning are the two most reported complications related to mesh [5].

A hallmark of mesh explants excised from women in areas of complications is the presence of marked deformations, including wrinkles, folds, and contraction [10–14]. *Ex vivo* mechanical tests and computational models corroborate instability of prolapse meshes with loading as evidenced by 1) collapsed pores and a reduction of porosity by 70–90% [15–17] and 2) mesh wrinkling [18]. Pore collapse, a planar deformation, is related to the pore geometry and the predominantly uniaxial loading conditions to which POP meshes are subjected. For polypropylene, a pore size of at least 1 mm is needed for tissue ingrowth, absence of bridging of the foreign body reaction between neighboring fibers, and avoidance of encapsulation [19]. Mesh-vagina explants removed from women with bothersome mesh-

related pain demonstrate crowding of fibers consistent with pore collapse, dense collagen encapsulation of the mesh, and are associated with an increased amount of TGF-β1, implicating fibrosis as a plausible mechanism for pain [20–22]. Mechanical activation of myofibroblasts, cells that secrete matrix and contract via the production of α-smooth muscle actin, underlies the mechanism of fibrosis [23, 24]. Secondly, mesh wrinkling (a non-planar deformation) results in a variable distribution of mesh on the vagina (i.e., areas with varied concentrations of mesh) likely resulting in regional stress variations [18]. In this situation, high-stress regions bear most of the load, while the adjacent regions experience little to no load, consistent with stress shielding, a plausible mechanism of mesh exposure. Collectively, the data to date suggest that the geometry a mesh assumes after tensioning and loading is an important factor to consider regarding patient outcomes, and mechanistic studies linking mesh deformation to complications are lacking.

The present study aimed to define the role of mesh deformation (pore collapse and wrinkles) in the pathogenesis of mesh complications. We hypothesized that two potential outcomes would occur due to the variable stresses imposed on the vagina by these deformations. In the first, the overall increase in mesh stiffness associated with deformed mesh would result in areas of stress shielding leading to profound tissue thinning and degradation – the mechanism of mesh exposure. In the second, areas of increased mesh burden (i.e., the amount of material in contact with the tissue), would also create areas of high tissue stress, and myofibroblast proliferation with matrix deposition to counteract the stress – a mechanism of fibrosis and pain. We further hypothesized that meshes with the greatest amount of deformation would produce the poorest outcomes.

2. Materials and Methods

2.1. Mesh

Restorelle, an ultra-lightweight mesh, was used in this study since its normal loading configuration is a square pore, which has been shown in *ex vivo* studies to be the most stable pore geometry [16] and had the least negative impact on the vagina when implanted by sacrocolpopexy *in vivo* [25–28]. Importantly, the square pore can be changed to a rhombus (referred to as a diamond) geometry by rotating the mesh 45°. In contrast to the square, the diamond pore is highly unstable, with over 90% reduction in porosity with minimal tension (10 N = ~2.2 lbs) [16]. To assess the impact of altered mesh geometry *in vivo*, Restorelle was implanted with three pre-defined pore geometries: 1) square pore (Stable), 2) diamond pore (Unstable), and 3) Predeformed pore (pores intentionally collapsed and mesh wrinkled prior to implantation). In the first two configurations, the mesh was implanted flat as opposed to the Predeformed configuration in which the mesh was intentionally wrinkled.

2.2. Animals

Thirty-eight nonhuman primates (NHPs), rhesus macaques (*Macaca mulatta*), underwent abdominal surgery utilizing methods approved by the University of Pittsburgh Institutional Animal Care and Use Committee (IACUC #19085471). A single animal served as the experimental unit. All animals were housed in standard cages with a 12-hour alternating light/dark cycle. NHPs were given water *ad libitum* and a scheduled monkey

diet supplemented with fresh fruit and vegetables. Age, weight, gravidity (number of pregnancies), and parity (number of vaginal deliveries) was collected for each NHP. A modified pelvic organ prolapse quantification (POP-Q) examination was performed, before and 12 weeks after surgery, on each animal (lightly sedated with ketamine hydrochloride: 10 mg/kg, xylazine hydrochloride: 0.5 mg/kg) as previously described [29].

2.3. Surgical procedures

Following intubation and laparotomy, 38 NHPs underwent a total hysterectomy and complete transection of level I (uterosacral ligaments) and II (paravaginal attachments) support, under anesthesia (isoflurane: 1–2.5%). Two straps of Restorelle mesh (Coloplast, Minneapolis, MN), 3 cm x 12 cm, were sutured to the anterior and posterior walls of the vagina of 30 NHPs by sacrocolpopexy, as previously described [25, 27]. Meshes were implanted with three predefined pore geometries: Stable (square, n=10), Unstable (diamond, n=10), and Predeformed (pores collapsed, mesh wrinkled, n=10). For the Stable pore geometry, Restorelle was implanted with the pores in the square configuration with respect to the loading direction, resulting in the pores remaining open with loading (Figure 1A). For the Unstable configuration, Restorelle was implanted with the pores in the diamond orientation, which was achieved by rotating the mesh 45º with respect to the loading direction, resulting in pore collapse primarily in the mesh bridge to the sacrum and at the apex of the vagina (Figure 1B). The mesh was sutured to the vagina so that it would remain flat with tensioning and loading for both the Stable and Unstable groups. For the Predeformed pore configuration, Restorelle was implanted with the pores in the diamond configuration; the pores were collapsed and the mesh was intentionally wrinkled prior to attaching it to the vagina (Figure 1C). The surgeon performing the surgery was blinded to the mesh configuration until the dissection for each mesh implantation was completed.

To standardize the amount of tension placed on the meshes, all meshes were tensioned to the sacrum at 10 N, using a spring scale. It is important to note that 10 N is within the physiological range but places tension on the mesh. Eight animals served as sham-operated controls, with no mesh implanted. All animals were given the appropriate anesthetics (ketamine hydrochloride: 10 mg/kg, xylazine hydrochloride: 0.5 mg/kg) and analgesics (buprenorphine hydrochloride: 0.03 mg/kg, meloxicam: 0.2 mg/kg) before, during, and after surgery (as per protocol IACUC #19085471) to reduce pain and distress. Additionally, all animals were monitored daily for signs of pain, distress, or well-being and weighed bi-weekly by laboratory and veterinarian staff. After 12 weeks, the mesh-vagina complexes (MVCs) or vagina alone (Sham) were harvested. Key structural components of the vagina were assessed using both the anterior and posterior vagina. Additionally, the contractile function (active mechanics) of the vagina was evaluated using the anterior vagina, and the posterior vagina was utilized to assess the structural integrity (passive properties) of the vagina. Importantly, for all subsequent studies, technicians and students performing the assays were blinded to the study aims and mesh groups.

2.4. Masson’s trichrome staining

To assess the overall morphology of the vagina, full-thickness samples of the anterior vagina were stained with Masson’s trichrome. Briefly, samples were fixed and sectioned at 7

μm. Sections were stained with trichrome stain AB and Hematoxylin Gill, No. 2 solutions (Sigma-Aldrich, St. Louis, MO, USA). Tissue sections were imaged using a Nikon Eclipse 90i microscope (Melville, NY, USA).

2.5. Immunofluorescence staining of smooth muscle, apoptosis, and myofibroblasts

Portions of the anterior vagina were embedded in optimal cutting temperature compound and cryosectioned (7 μm), with the sections cut perpendicularly to the vagina. Tissue sections were incubated overnight at 4°C with the primary antibody, mouse anti-α-smooth muscle actin (Sigma, St. Louis, MO), at a 1:100 dilution. Following overnight incubation, the secondary antibody, donkey anti-mouse conjugated with Alexa Flora 594 (Thermo Fisher Scientific, Waltham, MA), was applied (1:200 dilution), and cell apoptosis was labeled via the *in situ* terminal deoxynucleotidyl transferase-mediated dUTP nick-end labeling TUNEL assay (Roche, Branchburg, NJ, USA)[27]. Images were taken at 10X with a Nikon Eclipse 90i microscope (Melville, NY). The NIS-ELEMENTS AR3.2 (Nikon) software was utilized to quantify the:

1. area of the subepithelium, muscularis (smooth muscle), and adventitia
2. area of the tissue section
3. total number of cells within the subepithelium, muscularis, and adventitia
4. number of apoptotic cells within the subepithelium, muscularis, and adventitia
5. number and area of mesh fibers within the adventitia layer of mesh-implanted vaginas.

It is important to note that only those portions of the tissue section(s) that were full-thickness (i.e., all layers of the vagina represented – epithelium, subepithelium, muscularis, and adventitia) were analyzed. Additionally, the number of apoptotic cells within the epithelium and the area of the epithelium were excluded from the respective totals, given the high turnover and variability of the epithelial layer. Myofibroblasts were identified and quantified within the adventitial layer of the vagina, using α-smooth muscle actin [30] (labeling as described above) and the open source image-analysis software QuPath-0.2.3 (Queen's University, Belfast, Northern Ireland) [31], respectively. Briefly, in QuPath-0.2.3, the adventitia layer was outlined to define the region of interest. The cell detection tool (maximum area = 500 μm^2 and threshold = 20; default settings were used for all other parameters) was utilized to identify cells labeled with α-smooth muscle actin. All cells and tissues with non-myofibroblast morphology (e.g., blood vessels) were manually removed prior to quantifying the number of myofibroblasts.

2.6. Hydroxyproline assay

Total collagen content of lyophilized and papain digested (final concentration, 125 μg/ml) tissue samples was quantified with the hydroxyproline assay, using methods previously described [27, 32]. The experiment was repeated two times minimally for each animal. To estimate the total collagen content, it was assumed that hydroxyproline comprises 14% of the amino acid composition of collagen [27, 33]. The total collagen content was normalized to tissue dry weight.

2.7. 1,9-Dimethylmethylene blue assay

The amount of sulphated glycosaminoglycan (sGAG) in papain (final concentration, 125 μg/ml) -digested vaginal tissues was quantified using the 1,9-dimethylmethylene blue assay as previously described [27, 32]. The assay was repeated, at a minimum, in duplicate for each animal, and the amount of sGAG was normalized to tissue dry weight.

2.8. Mature elastin quantification

Ultrahigh performance liquid chromatography (UPLC) was used to quantify the amount of mature elastin within the samples as previously described [34]. It was assumed that isodesmosine and desmosine comprise 1.3% of mature elastin (by weight) [35]. Mature elastin was reported as the sum of the amount of desmosine and isodesmosine, normalized to the tissue dry weight.

2.9. Transforming growth factor-beta1 (TGF-β1) quantification

The total amount of TGF-β1 was quantified using a commercially available enzyme-linked immunosorbent assay (ELISA; R&D Systems, Minneapolis, MN). The activation step to quantify the amount of endogenous active TGF-β1was omitted; therefore, the amount of latent TGF-β1 was estimated by subtracting the amount of endogenous active TGF-β1 from the total amount. All samples were run in duplicate, with either 40 μg (total) or 60 μg (endogenous active) of protein per sample per assay. The amount of latent and active TGF-β1 was normalized to the amount of protein, quantified with the DC protein assay (Bio-Rad Laboratories, Hercules, CA).

2.10. Gelatin zymography for MMP-2

Protein concentration in each sample was measured via the DC protein assay (Bio-Rad, Hercules, CA). Substrate zymography, with 30 μg of protein per sample, was used to quantify the expression of pro- and active metalloproteinase-2. Experiments were carried out in duplicate using a pre-cast 10%-gelatin gel system (Invitrogen, Carlsbad, CA), as described previously [36].

2.11. ELISA for MMP-9 quantification

The active and proforms of MMP-9 are not clearly delineated using gelatin zymography [28]; therefore, the level of matrix degrading enzyme metalloproteinase-9 was measured using the Human MMP-9 Quantikine ELISA kit (R&D Systems Minneapolis, MN). Each sample was tested in duplicate with 40 μg (endogenous active) or 20 μg of protein per sample per assay. The ELISA was performed with and without activating the samples with amino-phenyl mercuric acetate (APMA) to quantify the amount of active and total enzyme present, respectively, from which the amount of proenzyme was calculated (pro = total – endogenous active). The amount of active and proenzyme was normalized to the amount of protein.

2.12. Collagenase activity

A collagenase activity assay with fluorescein isothiocyanate (FITC)-labeled telopeptide-free soluble bovine type I collagen (Chondrex, Redmond, WA) was used to measure total

collagenase activity as previously described [27]. A collagenase activator was not added to the samples; therefore, the assay measured total collagenase activity, including the tissue inhibitors of metalloproteinase contained within each sample. All samples were measured in duplicate and the collagenolytic activity was reported as units/ml where 1 unit equals the cleavage of 1 μg of collagen per minute.

2.13. Fluorokine assay for MMP-1 quantification

Enzyme activity of MMP-1 was quantitatively measured using the Human Active MMP-1 Fluorescent Assay kit (R&D Systems Minneapolis, MN). Samples were measured in duplicate and the assay was performed with and without activating the samples with APMA to discern endogenous active (40 μg of protein per sample per assay) and total enzyme (20 μg of protein per sample per assay) present, respectively. The pro-enzyme form of MMP-1 was obtained by subtracting the endogenous active from the total enzyme. The amount of active and proenzyme was normalized to the amount of protein.

2.14. Active mechanics

The contractile function of the vagina in the presence of mesh was assessed using a contractility assay as previously described [25]. Briefly, two strips (7 mm x 2 mm), oriented along the circumferential axis, were cut from the proximal (anterior) vagina and exposed to 120 mM potassium chloride (KCl), a muscle myofiber stimulant, within 30 minutes of tissue harvest. The maximum contractile force was averaged and normalized to tissue volume (mN/mm^3) to account for differences in the volume of the vaginal strips.

2.15. Passive mechanics

The structural integrity of the mesh implanted and Sham posterior vaginas was evaluated using ball-burst testing. The structural properties, stiffness (N/mm), load at failure (N), extension at failure (mm), and energy absorbed to failure (N*mm), of the MVCs and Sham vaginas were determined as previously described [25]. The same protocol was utilized to characterize the *ex vivo* structural properties of the Stable pore (square, n=5), Unstable pore (diamond, n=5), and Predeformed (pores collapsed and wrinkled, n=5) meshes to estimate the contributions of the vagina to the overall complex stiffness. Note, each mesh was preconfigured and tensioned to 10 N to mimic the surgical implantation dimensions and pore orientation prior to ball-burst testing. The stiffness of the tissue was estimated by subtracting the average *ex vivo* mesh stiffness from the total MVC stiffness utilizing assumptions as described previously [25].

2.16. Statistics

Sample size was calculated based on previously published data on the implantation of Restorelle (the mesh utilized in this study) and Gynemesh (Ethicon, a mesh that negatively impacts vaginal structure and function), in a flat configuration, onto the vagina of NHPs [25–27]. A power analysis revealed that eight animals per group would be needed to detect a 20% difference in the contractile function of the vagina (primary outcome) following implantation of flat versus deformed (pores collapsed and/or mesh wrinkled) mesh as compared to Sham with a power of 80% and α <0.05, using a two-tailed t-test. Kolmogorov-

Smirnov tests were used to determine normality. Differences between groups in normally distributed data were compared using one-way ANOVA followed by Dunnett t-tests or independent samples t-tests with a Bonferroni correction for multiple comparisons when appropriate. Kruskal-Wallis followed by Mann-Whitney tests with a Bonferroni correction, when appropriate, were used to assess non-parametric data and normally distributed data in which variance between groups was not equal. Categorical data was compared using Fisher's Exact. The associations among outcomes of interest were analyzed using linear regression or Spearman's correlation coefficients. All statistical analyses were performed using SPSS 26.0 statistical software (IBM, Armonk, NY). The significance level was set to $p<0.05$ unless otherwise specified.

3. Results

Animals were middle aged with similar weight, parity, and gravidity (Table 1). NHPs in the Stable group were significantly older (P=0.016) relative to Sham (Table 1). However, linear regression analysis revealed that age did not significantly impact the results of this study (P>0.05). Prior to surgery, one animal had Stage 2 (Stage 1 post-surgery) and one had Stage 4 (Stage 0 post-surgery) prolapse in the Unstable and Stable groups, respectively. Following surgery, four NHPs had Stage 2 prolapse in which the leading edge of the prolapse (in this case the anterior vaginal wall) descends to the level of the hymen (Sham n=3 and Unstable n=1, P=0.011). This is likely a result of surgical disruption of Level I and II support, which resulted in prolapse in some Sham animals, and elongation of the mesh bridge to the sacrum which occurs with pore collapse in the Unstable group. Additionally, one NHP in the Stable group was excluded, due to weight loss of unclear etiology, leaving a final sample size of Sham (n=8), Stable (n=9), Unstable (n=10), and Predeformed (n=10).

3.1. Mesh deformation

Qualitative assessment of the mesh-vagina complexes demonstrated that the meshes in the Stable group remained flat with normal tissue incorporated within the mesh pores (Figure 2). Meshes in the Unstable group also remained relatively flat, even in areas where the pores had collapsed (Figure 2). This contrasts with the Predeformed meshes which had both collapsed pores and wrinkles and was associated with poor quality tissue within the mesh pores (Figure 2). Additionally, Predeformed mesh-vagina complexes were significantly thicker than the Stable and Unstable complexes [Predeformed – 6.7 ± 1.7 vs Stable – 5.2 ± 0.6, P=0.021, and Unstable – 5.1 ± 1.0, P=0.013]. Quantifying the number of fibers within the vaginal adventitia (site of mesh implantation), more fibers were observed in the Predeformed configuration [61.0(35.8–203)] relative to the Stable [27.0(15.0–48.5), P=0.017] and Unstable configurations [(32.5(22.5–49.8), P=0.035)]. Similarly, the area of mesh fibers relative to vaginal adventitia area was also higher for the Predeformed configuration [17.0(5.9–28.4)] relative to Stable [4.1(2.5–9.6), P=0.017] and Unstable [6.1(3.4–13.4, P=0.035].

3.2. Gross appearance and vaginal morphology

Mesh exposures occurred in the Unstable (n=3) and Predeformed geometries (n=3), with most of the exposures occurring towards the apex of the vagina and 100% occurring

where the pores collapsed and the mesh wrinkled (Figure 3C-E). Despite implanting the Stable-pored meshes in a flat configuration, as stated previously, one of the Stable-pored meshes (n=1) wrinkled, which resulted in a mesh exposure (Figure 3C). However, not all areas of pore collapse and wrinkling led to a mesh exposure. On gross examination of the explanted mesh-vagina complexes in areas of deformed mesh, smoothing, with a complete loss of the vaginal rugae (i.e., vaginal flattening), were observed (Figure 3C-E). In addition, in many areas of deformed mesh, in the absence of exposure, a dense fibrotic capsule was observed (Figure 4, right image).

Profound thinning of the vagina was observed with mesh deformation (Figure 5, left image). Overall, the muscularis (smooth muscle) layer was the most impacted, particularly for the Predeformed group (Figure 5D). Specifically, the smooth muscle layer in the Predeformed group was disorganized, less densely packed, and had qualitatively smaller smooth muscle bundle sizes (Figure 5D). This contrasts with Sham in which well-organized layers of inner circular and outer longitudinal smooth muscle were observed (Figure 5A). Additionally, the Predeformed muscularis area was significantly less than Sham (P=0.042, Table 2). For the Stable group, there was some thinning of the smooth muscle layer, but overall, the organized architecture was preserved (Figure 5B). In the Unstable group, the appearance of the smooth muscle varied according to the geometry of the mesh. Where the mesh pores remained relatively open (distal vagina), the smooth muscle appeared more similar to the Stable group (Figure 5C). In areas where pores collapsed (vaginal apex), loosely packed, disorganized smooth muscle bundles were observed (not pictured). Labeling with α-smooth muscle actin confirmed the observations with trichrome (Supplemental Figure 1).

Normal tissue incorporation into the mesh pores was most apparent in the Stable (Figure 5B) and nondeformed areas of the Unstable (Figure 5C) groups and the least in the Predeformed group. There was minimal evidence of normal tissue incorporation with an excessive amount of matrix deposition, particularly in areas with a high mesh burden (Figure 5D) for the Predefomred group, which led to a significant increase in the area of the adventitia (overall, P=0.045, Table 2). Overall, the area of the subepithelium ($\rho = -0.423$, P=0.016) and muscularis ($\rho = -0.856$, $P < 0.001$) negatively correlated with the area of the adventitia, indicative of vaginal thinning with increasing mesh deformation, corroborating an inverse relationship between the amount of mesh in contact with the host (due to mesh deformation) and the thickness of the vagina.

Following mesh implantation, the number of apoptotic cells significantly increased with deformation in the muscularis (overall P=0.025, Table 3) and adventitia (overall P=0.029, Table 3). Apoptosis was highest in the Predeformed group, with 16x more apoptotic cells in the muscularis (vaginal smooth muscle layer) compared to Sham (P=0.009). Similarly, there were approximately 3x and 4x as many apoptotic cells in the adventitial layer in the Stable (P=0.009) and Predeformed (P=0.021) groups compared to Sham, respectively. The number of apoptotic cells within the subepithelium was not significantly different between layers (overall P=0.10, Table 3).

3.3. Structural components of the vagina

3.3.1. Total collagen, sGAG, mature elastin content, and collagenase activity

—Among the structural proteins investigated, collagen was the most impacted, with a significant decrease observed following the implantation of all mesh configurations (overall P=0.003). Specifically, a 32% reduction in the amount of collagen was observed in the Predeformed implanted vaginas compared to Sham (P=0.002, Figure 6). Mature elastin content, sGAG, and collagenase activity were not significantly different between groups (Figure 6).

3.3.2. Extracellular matrix degrading enzymes—Proteolytic activity was increased in the presence of mesh, specifically for the Unstable and Predeformed groups. The ratio of active to pro-enzyme MMP-2 was 162% higher for the Unstable group (P=0.005), 151% higher for the Predeformed group (P=0.033), and 77% higher for the Stable group (P=0.042) relative to Sham (Figure 6). Similarly, the ratio of the active to pro-enzyme form of MMP-9 for the Predeformed group was 3.8 (P=0.013) times greater than Sham (Figure 6). This result is largely driven by the 177% increase in active MMP-9 for the Predeformed group (P=0.014, data not shown). Active MMP-1 was also significantly higher in the Predeformed group as compared to Sham (P=0.014, Figure 6). No significant differences were observed in the amount of active MMP-2 (P=0.16), pro MMP-2 (P=0.73), pro MMP-9 (P=0.068), pro MMP-1 (P=0.18), nor the ratio of active to pro-enzyme (P=0.55) MMP-1. Collectively, the increased amounts of MMPs 1, 2, and 9 corroborate accelerated matrix degradation.

3.3.3. TGF-β1 quantification—TGF-β1 is a potent regulator of matrix turnover, and increased amounts of TGF-β1 are associated with myofibroblast proliferation and matrix deposition. Overall, the amount of active TGF-β1 for the mesh-implanted groups was significantly higher than Sham (P=0.020, Figure 6). Post hoc pairwise comparisons showed that active TGF-β1 was 1.5x higher for the Predeformed configuration relative to Sham (P=0.001, Figure 6). The amount of latent TGF-β1 nor the ratio of active to latent TGF-β1 was significantly different between groups (P>0.05 for both).

3.3.4. Myofibroblast quantification—Myofibroblasts are present during normal wound healing and undergo programmed apoptosis when healing is complete, typically over a period of 3–4 weeks. Persistence of myofibroblasts in a wound (i.e., failure of myofibroblast apoptosis) is indicative of an abnormal healing response [30, 37]. Myofibroblasts persisted at the site of mesh implantation in all groups. Specifically, the number of myofibroblasts increased with mesh deformation and was associated with abnormal extracellular matrix deposition and collagen deposition/fibrosis (Figure 7, Figure 8 left). Relative to Sham, there were 10.7 (P=0.031), 24.2 (P=0.010), and 103.8 (P=0.001) more myofibroblasts within the adventitia of the Stable, Unstable, and Predeformed configurations, respectively. Furthermore, the percentage of myofibroblasts (defined as the total number of myofibroblasts relative to the total number of cells) was significantly higher for the Predeformed group (~50 times higher, P=0.001) relative to Sham (Figure 8 right). Comparing across mesh groups, the percentage of myofibroblasts within the Predeformed adventitia was 8.5 times higher than the Stable configuration (P=0.010). Independent of the implantation configuration, the number of myofibroblasts was positively associated with

the number of mesh fibers within the adventitia (ρ=0.606, P<0.001), fiber area (ρ=0.618, P<0.001), and adventitia area (ρ=0.709, P<0.001).

3.4. Vaginal contractile function (Active mechanics)

Vaginal contractility in the presence of deformed mesh was markedly impaired (P=0.025). In response to 120 mM KCl, vaginal contractile function was reduced by 66% for the Predeformed configuration relative to Sham, P=0.015 (Figure 9). In the presence of the Stable configuration, the contractile response was also reduced 42% (P=0.11) compared to Sham. Similarly, the vaginal contractility of the Unstable configuration was not different from Sham (P=0.54).

3.5. Structural integrity of the vagina following mesh implantation (Passive mechanics)

3.5.1. Structural properties of mesh-vagina complexes—Rupture of the vagina and MVCs occurred at the point of contact with the steel-ball head for all samples tested. Overall, MVCs were stiffer (P=0.036), stronger (P=0.011), and tougher (i.e., required more energy to reach failure, P=0.021) relative to Sham, consistent with the mechanical behavior of mesh (Supplemental Table 1). Of note, the stiffness of the Predeformed MVCs was 81% higher relative to Sham (P=0.019). As expected, the introduction of mesh deformations increased the stiffness and strength of the mesh-vagina complex, associated with an increase in overall mesh burden (i.e., the amount of mesh in contact with the tissue).

3.5.2. Estimated vaginal stiffness contribution to overall MVC stiffness—The structural integrity of the vagina (i.e., the estimated contribution of the vagina to the overall MVC stiffness) was determined by subtracting the stiffness of the mesh alone (Supplemental Table 1) from the MVC stiffness (Supplemental Table 2), both obtained via ball-burst testing. Consistent with a degradative predominant stress-shielding response, the contribution of the vagina to the total stiffness of the MVC decreased with increasing mesh deformation (Figure 10). Specifically, the vagina accounted for only 22% of the Predeformed MVC stiffness, which is significantly less than the 80% (P<0.001) and 73% (P<0.001) estimated vaginal stiffness of the tissue in the Stable and Unstable MVCs, respectively. The observed decreases in stiffness suggest that the overall structural integrity of the vagina is compromised in the presence of pore collapse and mesh wrinkling.

4. Discussion

Until now, evidence that mesh deformations lead to complications *in vivo* was lacking. As a step towards defining mechanisms of mesh complications, we analyzed the *in vivo* impact of pore collapse (planar deformation) and mesh wrinkling (nonplanar deformation) on the biomechanical properties and structure of the vagina. For the first time, we have been able to reproduce what has been observed clinically for decades; that is, mesh deformations mechanistically lead to complications. Most interesting was our finding that mesh deformation led to two seemingly disparate host responses: 1) a maladaptive degradative remodeling response (the predominant response) characterized by decreased vaginal function and compromised structure, resulting in mesh exposure, and 2) myofibroblast proliferation and matrix deposition – a plausible mechanism of pain. Our

findings are consistent with variable stresses exerted on the tissue, with regions of low stress likely leading to stress shielding and mesh exposure and those of high stress inducing myofibroblast proliferation and matrix deposition. We observed that mesh exposures were associated with vaginal smoothing with a loss of vaginal rugae and thinning, similar to what is observed clinically. Collectively, these results provide direct evidence that mesh deformation is a contributing factor in the pathogenesis of mesh complications. They also corroborate the need to implant and maintain mesh in a flat configuration for improved patient outcomes. Furthermore, the results of this study demonstrate that implanting a lightweight mesh with a pore size > 1 mm and a favorable porosity will not be associated with good outcomes if the mesh wrinkles and the pores collapse with loading.

Pore collapse leads to inadequate tissue incorporation within the mesh pores, bridging fibrosis, and encapsulation, typical of mesh explants removed from patients experiencing complications [15–17]. Our finding that the Unstable diamond configuration had limited impact on tissue integration and the functional and structural properties of the vagina is likely driven by the pores remaining relatively open on the distal vagina and pore collapse occurring primarily on the proximal vagina (apex) and in the adjacent mesh bridge to the sacrum. A reduction in tension resulting from elongation, a consequence of pore collapse, in the Unstable configuration may also explain the lower impact of the Unstable configuration on the vagina. It is however important to note that in this group, animals in which increased pore collapse was observed on the vagina (vaginal apex and within the mesh bridge of the Unstable configuration), mesh exposures were observed. Clinically, it is possible that, in obese women or women with severe prolapse, higher loads will be placed on the mesh, resulting in considerably more pore collapse on the vaginal portion of the mesh (particularly for meshes with diamond or hexagon pore shapes), thereby increasing the risk of mesh complications. Future studies utilizing an alternative implantation and/or tensioning scheme that ensures the pores on the vagina are collapsed (without the mesh wrinkling) and implantation times beyond 12 weeks are needed to isolate the independent impact of pore collapse on the vagina.

Fibroblasts regulate extracellular matrix homeostasis and differentiate into myofibroblasts in response to chemical (e.g., TGF-β1) and mechanical (e.g., increased matrix stiffness) cues [38–40]. During normal wound healing, myofibroblasts proliferate, secrete collagen to stabilize the wound, and undergo programmed apoptosis once mechanical homeostasis is achieved. Failure of myofibroblast apoptosis leads to proliferation, increased matrix deposition, fibrosis, and tissue contraction [41]. The persistence of myofibroblasts in the adventitia of the vagina 12-weeks following mesh implantation, as observed in this study, is atypical of the normal wound healing response and likely a mechanical response. Mechanical tension has been identified as a regulator of the fibroblast to myofibroblast transition in both *in vitro* and *in vivo* models of skin wound healing [39, 42]. Similarly, the composition of the extracellular matrix (ECM) as well as the stiffness have been implicated as regulators of the vaginal fibroblast to myofibroblast transition using an *in vitro* model [43]. Our findings in the present *in vivo* study that 1) the stiffest mesh configurations, Unstable and Predeformed, were associated with myofibroblast proliferation and matrix deposition and 2) TGF-β1 was increased for Predeformed supports the role of stiffness and ECM composition in vaginal fibroblast differentiation. Additionally, the positive correlation

between the number of myofibroblasts and 1) the number of mesh fibers and 2) fiber area, independent of the mesh configuration, suggests that the myofibroblast response in the current study is mechanical.

Previous studies have identified fibrosis as the likely mechanism of pain with increased collagen deposition and positive associations between 1) interleukin-10 (a pro-fibrotic cytokine) and M2 (pro-remodeling) macrophages and 2) TGF-β1 and collagen type I observed in mesh explants removed for pain [20, 21]. Despite mesh removal, for some patients pain persists and TGF-β1 levels remain high [44]. Similar to breast implants in which myofibroblasts are linked to capsular contracture [45], the persistence of pain despite mesh removal is likely a result of contraction of the myofibroblasts [41] that remain in the area and the continued conversion of fibroblasts to myofibroblasts in response to TGF-β1 as well as increased mechanical stress. The presence of myofibroblasts and high levels of TGF-β1 in this study suggest that pathologic myofibroblast proliferation is the likely mechanism of pain following mesh implantation and future studies analyzing myofibroblasts in and adjacent to mesh explants removed for pain are warranted.

Mesh exposure is one of the most reported complications, occurring in roughly 10.5% of transabdominal procedures and 10–20% of transvaginal procedures [5, 7, 46–48]. Clinically, mesh explants removed for complications are often markedly deformed bearing little resemblance to their appearance at the time of implantation [10–14]. Similarly, our observation that mesh exposures were observed in areas of deformed mesh and in these areas the vagina was markedly thinned with increased proteolytic activity, decreased structural proteins, and compromised function, strongly implicate mesh deformation and tissue degradation as the underlying mechanisms of mesh exposure. Our findings corroborate previous studies in which 1) mesh explants removed from patients for the indication of exposure were associated with increased cytotoxic T cells and pro-MMP-9, evidence of tissue degradation [20, 21], and 2) mesh wrinkles led to vaginal thinning and mesh exposure in a rabbit lumbar colpopexy model [49]. Previous studies utilizing a nonhuman primate sacrocolpopexy model [25–27, 50] and an ovine transvaginal model [51] have also implicated mesh stiffness as a contributing factor to tissue degradation and mesh exposure. The results of this study support that mesh stiffness is a critical contributing factor given that with each deformation introduced (collapsed pores and then collapsed pores and wrinkles), the stiffness of the implanted product increased and so did the incidence of mesh exposures. Thus, unlike previous studies, increased mesh stiffness in the current study was a direct effect of each mesh deformation, which further supports a mechanistic basis of mesh deformation leading to mesh exposure.

The utilization of the same mesh in three predefined configurations to prove our hypothesis is a major strength of this study. By using the same mesh, the impact of mesh deformation can be assessed independently of mesh textile properties. The mesh utilized in this study is typically associated with good outcomes when implanted in the intended loading direction (square) [25–27, 50]. Thus, the results of this study can be attributed to the manipulations utilized and the experimental conditions rather than to the mesh itself. Additionally, the nonhuman primate is currently the gold standard for studying the impact of mesh on the

vagina, with results that are easily translatable to humans. The ability to reproduce mesh complications that occur in humans further strengthens this study.

Despite its strengths, this study is not without limitations. First, the NHP is an expensive model and a limited resource; hence this study had a small sample size, and only one time point was assessed. Additionally, the contractile function of the smooth muscle was indirectly measured using a vaginal contractility assay. Although limiting, the smooth muscle layer was not isolated as separating this layer would result in tissue damage. Furthermore, to simulate *in vivo* conditions (i.e., the ability of the smooth muscle to contract in the presence of mesh) it was important to keep the smooth muscle layer (i.e., the tissue) intact. Although, mesh wrinkling results in an uneven distribution of mesh fibers and regional increases in mesh burden, which subsequently results in nonuniform stress distributions placed on the vagina [18], in this study we were not able to definitively assess the local stress distributions throughout the mesh-vagina complexes. Samples for each analysis were taken from the same relative location; however, the distribution of mesh (and ultimately stress) likely varied. Thus, the location from which samples were taken for analysis possibly influence the results. This was particularly observed when comparing the results of relatively flat and evenly distributed mesh fibers versus deformed (collapsed pores and/or wrinkled) meshes. Future studies will inform the impact of the variable stress distribution imposed by mesh deformation on the vaginal host response.

Stress shielding, associated with degradation, and collectively, the increased level of TGF-β1 and myofibroblast proliferation, consistent with fibrosis, are competing phenomena that occurred simultaneously in this study, particularly within the Predeformed configuration. The presence of these opposing biologic processes is also a likely result of sampling location. In future studies, we aim to 1) use a technique (such as atomic force microscopy) that will aid our identification of areas of high and low stresses and their independent impact on the vagina and 2) to assess changes in vaginal extracellular matrix within these regions. Additionally, all meshes were placed on high tension (10 N). It is possible that tension could be a major contributor to myofibroblast proliferation. In other words, the increased tension could stimulate the fibroblast-to-myofibroblast transition and cause the myofibroblasts to align to resist tension. In future studies, deformed mesh will be implanted onto the vagina in the absence of tension to determine the impact of tension on myofibroblast proliferation. Such a study would also elucidate the impact of tension on the overall structure and function of the vagina given that mesh deformation is often a consequence of mesh tensioning.

Lastly, introducing pore collapse and wrinkles alters the porosity of the mesh configurations which consequently affects the amount of mesh in contact with the vagina and the stiffness of the mesh. The Predeformed mesh configuration therefore was associated with more mesh implanted and was stiffer, likely driving the heightened foreign body response (i.e., the maladaptive remodeling response) observed with the Predeformed configuration. It is nearly impossible to change one property of a mesh without changing another, as the structural properties of stiffness, load at failure, and energy absorbed to failure all are correlated with mesh stiffness and porosity [52]. Thus, we focused on mesh deformation and future studies, will aim to understand the role of the local mechanical environment on the tissue-remodeling response.

5. Conclusions

In summary, this study examined the *in vivo* impact of mesh deformation (i.e., pore collapse and mesh wrinkling) on the functional and structural properties of the vagina. For the first time, collapsed pores and wrinkling of a single type of mesh reproduced mesh exposures in a highly relevant animal model *in vivo* and were associated with a maladaptive remodeling response. The results of this study corroborate mesh deformation as a mechanism leading to mesh exposure and myofibroblast proliferation as a likely mechanism of pain, confirming that mesh implantation in a flat configuration with open pores is a critical factor in reducing complications in mesh-augmented surgeries.

Supplementary Material

Refer to Web version on PubMed Central for supplementary material.

Acknowledgements

The authors are grateful for the financial support provided by the National Institutes of Health R01 HD083383 grant funds to PAM and Steven D. Abramowitch, PhD (Department of Bioengineering, University of Pittsburgh). Research efforts for this publication were also supported by the National Center for Advancing Translational Sciences of the National Institutes of Health under award no. TL1TR001858 scholar funds to KMK. These studies were also supported by NIH/ORWH Building Interdisciplinary Research Careers in Women's Health (BIRWCH) K12HD043441 scholar funds to KMK. The content is solely the responsibility of the authors and does not necessarily represent the official views of the National Institutes of Health. Additionally, support was provided by the Magee-Womens Research Institute and Foundation Postdoctoral Fellowship Program scholar funds to KMK. The authors would like to thank Dr. Naoki Yoshimura, MD, PhD (Professor of Urology, Pharmacology, and Cell Biology, University of Pittsburgh), for allowing us to use the organ bath system to collect the contractility data reported; Dr. Robert Powers, PhD (Department of Obstetrics, Gynecology & Reproductive Sciences, University of Pittsburgh), for his assistance in the analysis of mature elastin; Dr. Leslie Meyn, PhD (Department of Obstetrics, Gynecology & Reproductive Sciences, University of Pittsburgh), for her assistance with statistical analysis; and Dr. Deanna C.E. Sinex, PhD, for her contributions to ball-burst testing. Lastly, the authors would like to thank Shaniel Bowen (PhD Student, Department of Bioengineering, University of Pittsburgh) for her artistic contributions to the graphical abstract.

Data Availability

The raw/processed data required to reproduce these findings cannot be shared at this time as the data also forms part of an ongoing study.

References

[1]. Samuelsson EC, Victor A, Tibblin G, Svardsudd KF, Signs of genital prolapse in a Swedish population of women 20 to 59 years of age and possible related factors, American Journal of Obstetrics and Gynecology 180(2 I) (1999) 299–305. [PubMed: 9988790]

[2]. Wu JM, Matthews CA, Conover MM, Pate V, Jonsson Funk M, Lifetime risk of stress urinary incontinence or pelvic organ prolapse surgery, Obstetrics and Gynecology 123(6) (2014) 1201–1206. [PubMed: 24807341]

[3]. Barber MD, Brubaker L, Burgio KL, Richter HE, Nygaard I, Weidner AC, Menefee SA, Lukacz ES, Norton P, Schaffer J, Nguyen JN, Borello-France D, Goode PS, Jakus-Waldman S, Spino C, Warren LK, Gantz MG, Meikle SF, Comparison of 2 transvaginal surgical approaches and perioperative behavioral therapy for apical vaginal prolapse: The OPTIMAL randomized trial, JAMA - Journal of the American Medical Association 311(10) (2014) 1023–1034. [PubMed: 24618964]

[4]. Jelovsek JE, Barber MD, Norton P, Brubaker L, Gantz M, Richter HE, Weidner A, Menefee S, Schaffer J, Pugh N, Meikle S, Effect of uterosacral ligament suspension vs sacrospinous ligament fixation with or without perioperative behavioral therapy for pelvic organ vaginal prolapse on surgical outcomes and prolapse symptoms at 5 years in the OPTIMAL randomized clinical trial, JAMA - Journal of the American Medical Association 319(15) (2018) 1554–1565. [PubMed: 29677302]

[5]. U.S.F.a.D. Administration, Surgical Mesh for Treatment of Women with Pelvic Organ Prolapse and Stress Urinary Incontinence: FDA Executive Summary, 2011.

[6]. Gupta P, Ehlert M, Bartley J, Gilleran J, Killinger KA, Boura JA, Nagaraju P, Fischer M, Perioperative Outcomes, Complications, and Efficacy of Robotic-Assisted Prolapse Repair: A Single Institution Study of 196 Patients, Female pelvic medicine & reconstructive surgery 24(6) (2018).

[7]. Nygaard I, Brubaker L, Zyczynski HM, Cundiff G, Richter H, Gantz M, Fine P, Menefee S, Ridgeway B, Visco A, Warren LK, Zhang M, Meikle S, Long-term outcomes following abdominal sacrocolpopexy for pelvic organ prolapse, Jama 309(19) (2013) 2016–24. [PubMed: 23677313]

[8]. Osmundsen BC, Clark A, Goldsmith C, Adams K, Denman MA, Edwards R, Gregory WT, Mesh erosion in robotic sacrocolpopexy, Female pelvic medicine & reconstructive surgery 18(2) (2012) 86–8. [PubMed: 22453317]

[9]. Manodoro, Endo M, Uvin P, Albersen M, Vláčil J, Engels A, Schmidt B, De Ridder D, Feola A, Deprest J, Graft-related complications and biaxial tensiometry following experimental vaginal implantation of flat mesh of variable dimensions, BJOG: An International Journal of Obstetrics and Gynaecology 120(2) (2013) 244–250. [PubMed: 23240803]

[10]. Caquant F, Collinet P, Debodinance P, Berrocal J, Garbin O, Rosenthal C, Clave H, Villet R, Jacquetin B, Cosson M, Safety of Trans Vaginal Mesh procedure: Retrospective study of 684 patients, Journal of Obstetrics and Gynaecology Research 34(4) (2008) 449–456. [PubMed: 18937698]

[11]. Feiner B, Maher C, Vaginal mesh contraction: Definition, clinical presentation, and management, Obstetrics and Gynecology 115(2 PART 1) (2010) 325–330. [PubMed: 20093906]

[12]. Svabik K, Martan A, Masata J, El-Haddad R, Hubka P, Pavlikova M, Ultrasound appearances after mesh implantation-- evidence of mesh contraction or folding?, Int Urogynecol J 22(5) (2011) 529–33. [PubMed: 20976440]

[13]. Javadian P, Quiroz LH, Shobeiri SA, In Vivo Ultrasound Characteristics of Vaginal Mesh Kit Complications, Female pelvic medicine & reconstructive surgery 23(2) (2017).

[14]. Rogowski A, Bienkowski P, Tosiak A, Jerzak M, Mierzejewski P, Baranowski W, Mesh retraction correlates with vaginal pain and overactive bladder symptoms after anterior vaginal mesh repair, International Urogynecology Journal and Pelvic Floor Dysfunction 24(12) (2013) 2087–2092.

[15]. Barone WR, Knight KM, Moalli PA, Abramowitch SD, Deformation of Transvaginal Mesh in Response to Multiaxial Loading, J Biomech Eng 141(2) (2019).

[16]. Barone WR, Moalli PA, Abramowitch SD, Textile properties of synthetic prolapse mesh in response to uniaxial loading, American Journal of Obstetrics and Gynecology 215(3) (2016) 326.e1–326.e9. [PubMed: 27001219]

[17]. Otto J, Kaldenhoff E, Kirschner-Hermanns R, Mühl T, Klinge U, Elongation of textile pelvic floor implants under load is related to complete loss of effective porosity, thereby favoring incorporation in scar plates, Journal of Biomedical Materials Research - Part A 102(4) (2014) 1079–1084. [PubMed: 23625516]

[18]. Barone WR, Amini R, Maiti S, Moalli PA, Abramowitch SD, The impact of boundary conditions on surface curvature of polypropylene mesh in response to uniaxial loading, Journal of Biomechanics 48(9) (2015) 1566–1574. [PubMed: 25843260]

[19]. Klinge U, Klosterhalfen B, Birkenhauer V, Junge K, Conze J, Schumpelick V, Impact of polymer pore size on the interface scar formation in a rat model, Journal of Surgical Research 103(2) (2002) 208–214. [PubMed: 11922736]

[20]. Nolfi AL, Brown BN, Liang R, Palcsey SL, Bonidie MJ, Abramowitch SD, Moalli PA, Host response to synthetic mesh in women with mesh complications, American Journal of Obstetrics and Gynecology 215(2) (2016) 206.e1–206.e8. [PubMed: 27094962]

[21]. Tennyson L, Rytel M, Palcsey S, Meyn L, Liang R, Moalli P, Characterization of the T-cell response to polypropylene mesh in women with complications, American Journal of Obstetrics and Gynecology 220(2) (2019) 187.e1–187.e8. [PubMed: 30419195]

[22]. Artsen AM, Rytel M, Liang R, King GE, Meyn L, Abramowitch SD, Moalli PA, Mesh induced fibrosis: The protective role of T regulatory cells, Acta biomaterialia 96 (2019) 203–210. [PubMed: 31326666]

[23]. Hinz B, The role of myofibroblasts in wound healing, Curr Res Transl Med 64(4) (2016) 171–177. [PubMed: 27939455]

[24]. Noskovicova N, Schuster R, van Putten S, Ezzo M, Koehler A, Boo S, Coelho NM, Griggs D, Ruminski P, McCulloch CA, Hinz B, Suppression of the fibrotic encapsulation of silicone implants by inhibiting the mechanical activation of profibrotic TGF-β, Nature Biomedical Engineering (2021).

[25]. Feola A, Abramowitch S, Jallah Z, Stein S, Barone W, Palcsey S, Moalli P, Deterioration in biomechanical properties of the vagina following implantation of a high-stiffness prolapse mesh, BJOG: An International Journal of Obstetrics and Gynaecology 120(2) (2013) 224–232. [PubMed: 23240801]

[26]. Jallah Z, Liang R, Feola A, Barone W, Palcsey S, Abramowitch SD, Yoshimura N, Moalli P, The impact of prolapse mesh on vaginal smooth muscle structure and function, BJOG : an international journal of obstetrics and gynaecology 123(7) (2016) 1076–85. [PubMed: 26301457]

[27]. Liang R, Abramowitch S, Knight K, Palcsey S, Nolfi A, Feola A, Stein S, Moalli PA, Vaginal degeneration following implantation of synthetic mesh with increased stiffness, BJOG: An International Journal of Obstetrics and Gynaecology 120(2) (2013) 233–243. [PubMed: 23240802]

[28]. Liang R, Zong W, Palcsey S, Abramowitch S, Moalli PA, Impact of prolapse meshes on the metabolism of vaginal extracellular matrix in rhesus macaque, American Journal of Obstetrics and Gynecology 212(2) (2015) 174.e1–174.e7. [PubMed: 25128444]

[29]. Feola A, Abramowitch S, Jones K, Stein S, Moalli P, Parity negatively impacts vaginal mechanical properties and collagen structure in rhesus macaques, American Journal of Obstetrics and Gynecology 203(6) (2010) 595.e1–595.e8.

[30]. Tomasek JJ, Gabbiani G, Hinz B, Chaponnier C, Brown RA, Myofibroblasts and mechano-regulation of connective tissue remodelling, Nature reviews. Molecular cell biology 3(5) (2002) 349–63. [PubMed: 11988769]

[31]. Bankhead P, Loughrey MB, Fernández JA, Dombrowski Y, McArt DG, Dunne PD, McQuaid S, Gray RT, Murray LJ, Coleman HG, James JA, Salto-Tellez M, Hamilton PW, QuPath: Open source software for digital pathology image analysis, Scientific Reports 7(1) (2017) 16878. [PubMed: 29203879]

[32]. Knight K, King GE, Palcsey SL, Artsen AM, Abramowitch SD, Moalli PA, A soft elastomer alternative to polypropylene for pelvic organ prolapse repair: a preliminary study, International Urogynecology Journal (In press).

[33]. Neuman RE, Logan MA, The determination of hydroxyproline, The Journal of biological chemistry 184(1) (1950) 299–306. [PubMed: 15421999]

[34]. Liang R, Knight K, Easley D, Palcsey S, Abramowitch S, Moalli PA, Towards rebuilding vaginal support utilizing an extracellular matrix bioscaffold, Acta biomaterialia (2017).

[35]. Covault HP, Lubrano T, Dietz AA, Rubinstein HM, Liquid-chromatographic measurement of elastin, Clinical Chemistry 28(7) (1982) 1465–1468. [PubMed: 7083557]

[36]. Moalli PA, Shand SH, Zyczynski HM, Gordy SC, Meyn LA, Remodeling of vaginal connective tissue in patients with prolapse, Obstetrics and Gynecology 106(5 I) (2005) 953–963. [PubMed: 16260512]

[37]. Baum J, Duffy HS, Fibroblasts and myofibroblasts: what are we talking about?, J Cardiovasc Pharmacol 57(4) (2011) 376–379. [PubMed: 21297493]

[38]. D'Urso M, Kurniawan NA, Mechanical and Physical Regulation of Fibroblast-Myofibroblast Transition: From Cellular Mechanoresponse to Tissue Pathology, Frontiers in bioengineering and biotechnology 8 (2020) 609653–609653. [PubMed: 33425874]

[39]. Hinz B, Mastrangelo D, Iselin CE, Chaponnier C, Gabbiani G, Mechanical tension controls granulation tissue contractile activity and myofibroblast differentiation, Am J Pathol 159(3) (2001) 1009–20. [PubMed: 11549593]

[40]. Arora PD, Narani N, McCulloch CA, The compliance of collagen gels regulates transforming growth factor-beta induction of alpha-smooth muscle actin in fibroblasts, Am J Pathol 154(3) (1999) 871–82. [PubMed: 10079265]

[41]. Li B, Wang JHC, Fibroblasts and myofibroblasts in wound healing: force generation and measurement, J Tissue Viability 20(4) (2011) 108–120. [PubMed: 19995679]

[42]. Rolin G.l., Binda D, Tissot M, Viennet C, Saas P, Muret P, Humbert P, In vitro study of the impact of mechanical tension on the dermal fibroblast phenotype in the context of skin wound healing, Journal of Biomechanics 47(14) (2014) 3555–3561. [PubMed: 25267573]

[43]. Ruiz-Zapata AM, Heinz A, Kerkhof MH, van de Westerlo-van Rijt C, Schmelzer CEH, Stoop R, Kluivers KB, Oosterwijk E, Extracellular Matrix Stiffness and Composition Regulate the Myofibroblast Differentiation of Vaginal Fibroblasts, Int J Mol Sci 21(13) (2020) 4762.

[44]. Artsen AM, Liang R, Meyn L, Rytel M, Palcsey S, Abramowitch SD, Moalli PA, T regulatory cells and TGF-β1: Predictors of the host response in mesh complications, Acta biomaterialia 115 (2020) 127–135. [PubMed: 32771596]

[45]. Hwang K, Sim HB, Huan F, Kim DJ, Myofibroblasts and Capsular Tissue Tension in Breast Capsular Contracture, Aesthetic Plastic Surgery 34(6) (2010) 716–721. [PubMed: 20512331]

[46]. Halaska M, Maxova K, Sottner O, Svabik K, Mlcoch M, Kolarik D, Mala I, Krofta L, Halaska MJ, A multicenter, randomized, prospective, controlled study comparing sacrospinous fixation and transvaginal mesh in the treatment of posthysterectomy vaginal vault prolapse, American Journal of Obstetrics & Gynecology 207(4) (2012) 301.e1–301.e7. [PubMed: 23021692]

[47]. Jacquetin B, Hinoul P, Gauld J, Fatton B, Rosenthal C, Clavé H, Garbin O, Berrocal J, Villet R, Salet-Lizée D, Debodinance P, Cosson M, Total transvaginal mesh (TVM) technique for treatment of pelvic organ prolapse: a 5-year prospective follow-up study, International Urogynecology Journal 24(10) (2013) 1679–1686. [PubMed: 23563891]

[48]. Nieminen K, Hiltunen R, Takala T, Heiskanen E, Merikari M, Niemi K, Heinonen PK, Outcomes after anterior vaginal wall repair with mesh: a randomized, controlled trial with a 3 year follow-up, American Journal of Obstetrics & Gynecology 203(3) (2010) 235.e1–235.e8. [PubMed: 20494332]

[49]. Knight KM, Artsen AM, Routzong MR, King GE, Abramowitch SD, Moalli PA, New Zealand white rabbit: a novel model for prolapse mesh implantation via a lumbar colpopexy, International Urogynecology Journal 31(1) (2020) 91–99. [PubMed: 31418044]

[50]. Shaffer RM, Liang R, Knight K, Carter-Brooks CM, Abramowitch S, Moalli PA, Impact of polypropylene prolapse mesh on vaginal smooth muscle in rhesus macaque, American Journal of Obstetrics and Gynecology (2019).

[51]. Emmerson S, Mukherjee S, Melendez-Munoz J, Cousins F, Edwards SL, Karjalainen P, Ng M, Tan KS, Darzi S, Bhakoo K, Rosamilia A, Werkmeister JA, Gargett CE, Composite mesh design for delivery of autologous mesenchymal stem cells influences mesh integration, exposure and biocompatibility in an ovine model of pelvic organ prolapse, Biomaterials 225 (2019) 119495. [PubMed: 31606680]

[52]. Feola A, Barone W, Moalli P, Abramowitch S, Characterizing the ex vivo textile and structural properties of synthetic prolapse mesh products, International Urogynecology Journal and Pelvic Floor Dysfunction 24(4) (2013) 559–564.

Statement of Significance

Pain and exposure are the two most reported complications associated with the use of polypropylene mesh in urogynecologic procedures. Most meshes have unstable geometries as evidenced by pore collapse and wrinkling after tensioning *ex vivo*, recapitulating what is observed in meshes excised from women with complications *in vivo*. We demonstrate that collapsed pores and wrinkling results in two distinct responses 1) mesh exposure associated with tissue degradation and atrophy and 2) myofibroblast proliferation and matrix deposition consistent with fibrosis, a tissue response associated with pain. In conclusion, mesh deformation leads to areas of tissue degradation and myofibroblast proliferation, the likely mechanisms of mesh exposure and pain, respectively. These data corroborate that mesh implantation in a flat configuration with open pores is a critical factor for reducing complications in mesh-augmented surgeries.

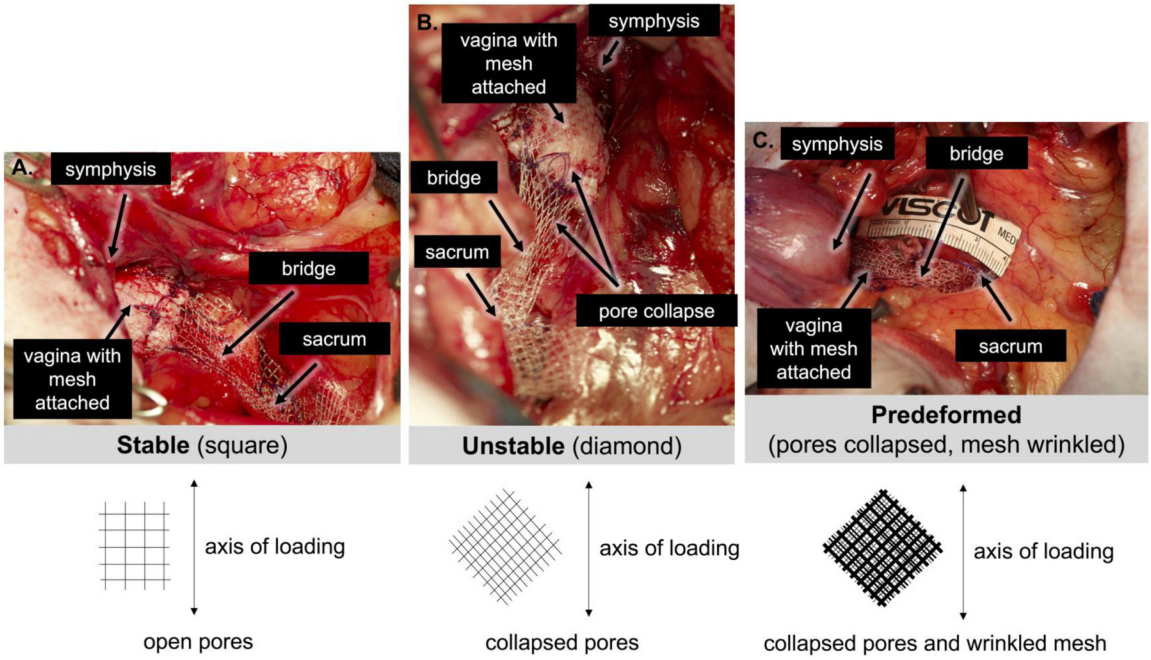

Figure 1: *In vivo* live images of Restorelle implanted in 3 different geometries

1) square pore, a **Stable** configuration (A), in which the pores stay open on the vagina with loading; 2) diamond pores, an **Unstable** configuration (B), in which the pores collapse, primarily in the mesh bridge to the sacrum and at the vaginal apex; 3) **Predeformed**, the most unstable configuration, achieved by allowing the pores to collapse and the mesh to wrinkle prior to implantation (C). Bottom schematics depict the orientation of the pores on the vagina with respect to the loading direction. Note: due to the 2D nature of the image, wrinkling of the mesh is not depicted in Predeformed schematic. Position of the pubic symphysis, vagina, mesh, mesh bridge to the sacrum, and sacrum are shown.

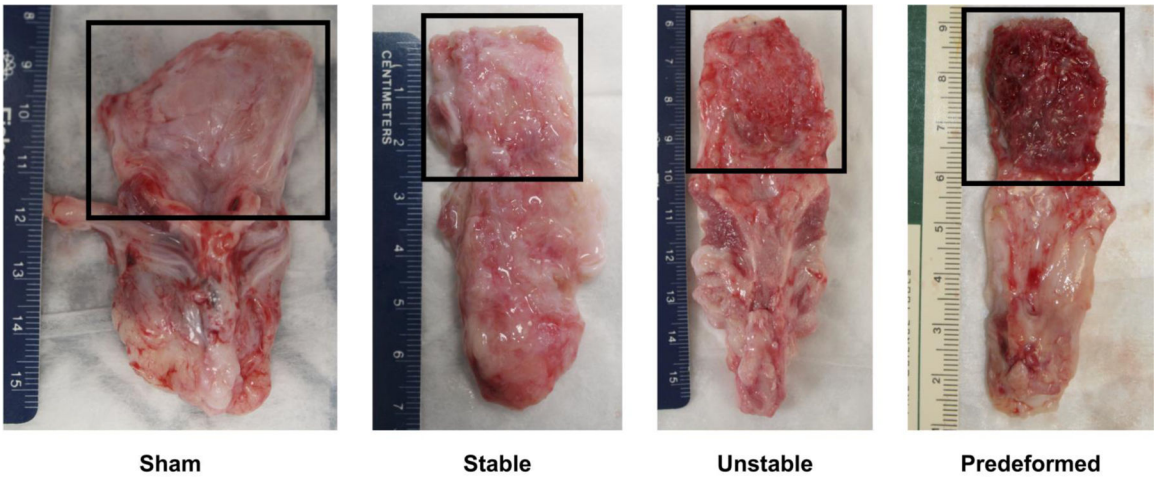

Figure 2: Mesh-vagina complex explants.

Exemplar mesh-vagina complex explants depicting the adventitial side of the vagina following sham surgery (no mesh) and the implantation of Stable, Unstable, and Predeformed. The grafted region is highlighted within the box. The mesh remained relatively flat with tissue incorporated within the mesh pores for the Stable and Unstable configurations whereas the mesh was wrinkled with poor quality tissue into the mesh for the Predeformed configuration.

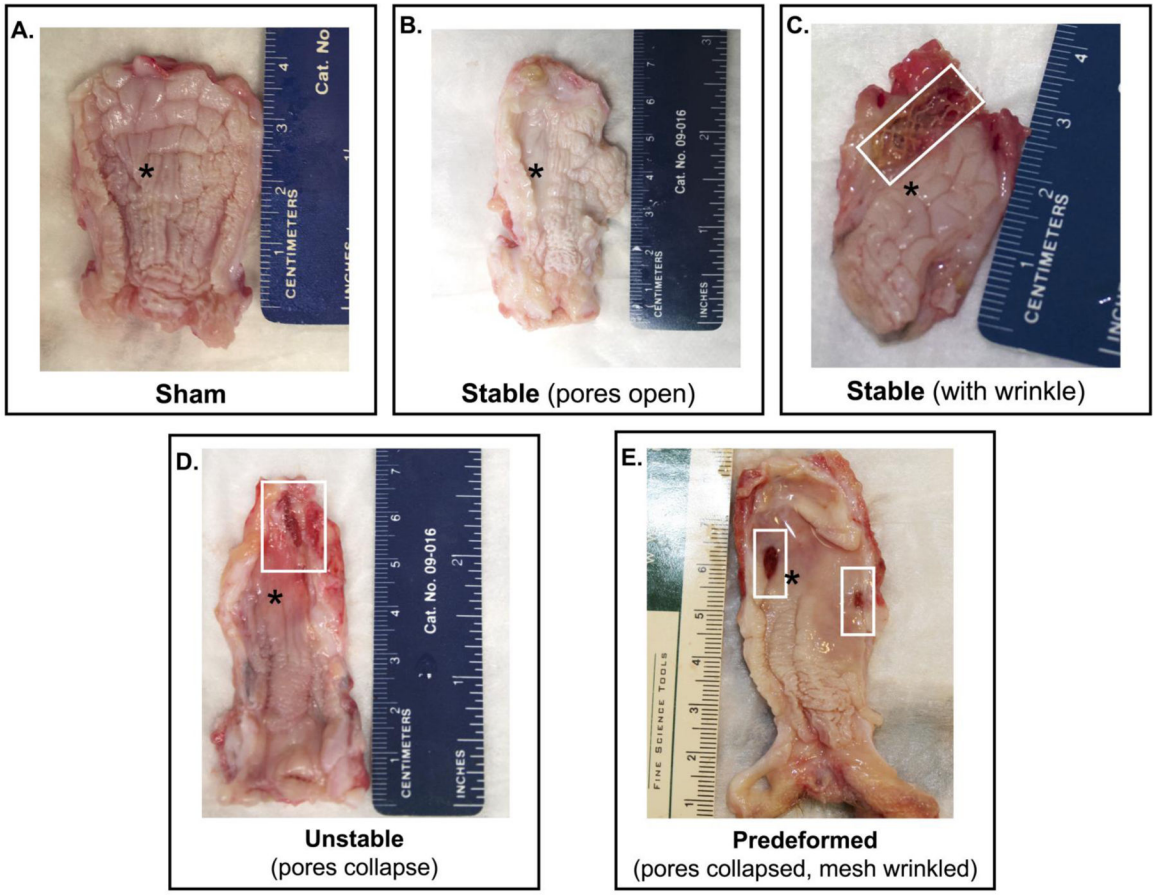

Figure 3: Mesh deformations reproduce mesh complications.

The luminal or epithelial side of the vagina at 12 weeks after surgery demonstrates that 1) deformations successfully reproduced mesh exposures, and 2) the degree of disruption of normal vaginal structure increased with increased deformations. Mesh exposures were most prevalent in the Unstable and Predeformed groups. Proof of this principle is shown in C, a specimen in which a wrinkle was incidentally introduced due to loss of a fixation suture. In the area of the wrinkle, a mesh exposure is observed. Mesh exposures were associated with a loss of rugae (*) or vaginal “smoothing,” which was most pronounced in the Predeformed configuration relative to Sham.

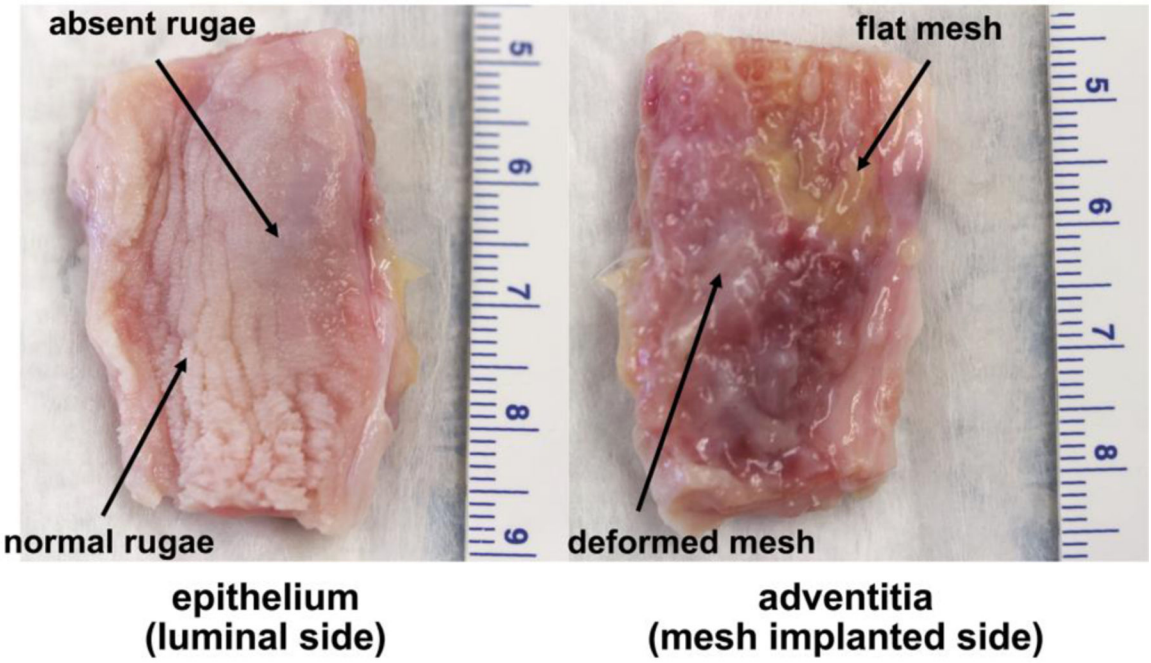

Figure 4: Profound morphological changes correspond to areas of mesh deformation.

Images of the vaginal epithelium and adventitia of the same mesh-vagina complex from the Predeformed group 12 weeks after surgery. An area where the mesh remained flat after loading is adjacent to an area of pore collapse and wrinkling. In the area where the mesh is flat, the vaginal rugae are normal but are noticeably absent in the areas where the mesh is deformed (right image). Dense fibrotic encapsulation (within the adventitia) is observed in the area of deformed mesh.

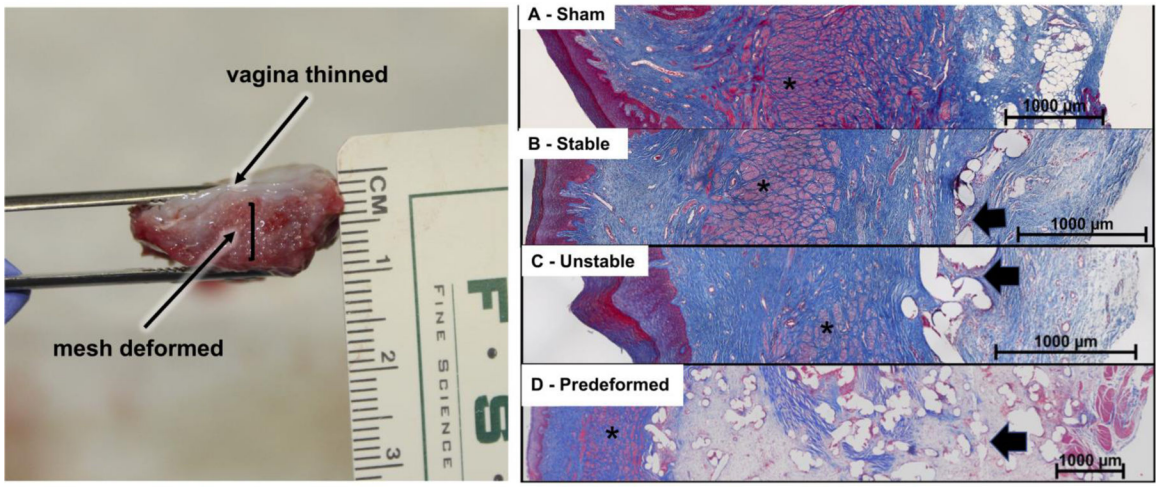

Figure 5: Deformed mesh results in vaginal thinning consistent with stress shielding.

Lateral view of a Predeformed mesh-vagina complex demonstrating dramatic vaginal thinning over an area of deformed mesh (**left**). Representative Masson's trichrome images of A) Sham, B) Stable, C) Unstable, and D) Predeformed configurations, demonstrating progressively increased crowding of mesh fibers with pore collapse in the Unstable configuration and pore collapse and wrinkling in the Predeformed group. Also apparent is marked thinning of the vagina, especially the smooth muscle layer (*), particularly in the Predeformed group, in which a high mesh burden, minimal tissue incorporation, and excessive matrix deposition (evidenced by faint pink staining within the adventitia layer) between the mesh pores (arrow) was observed (D).

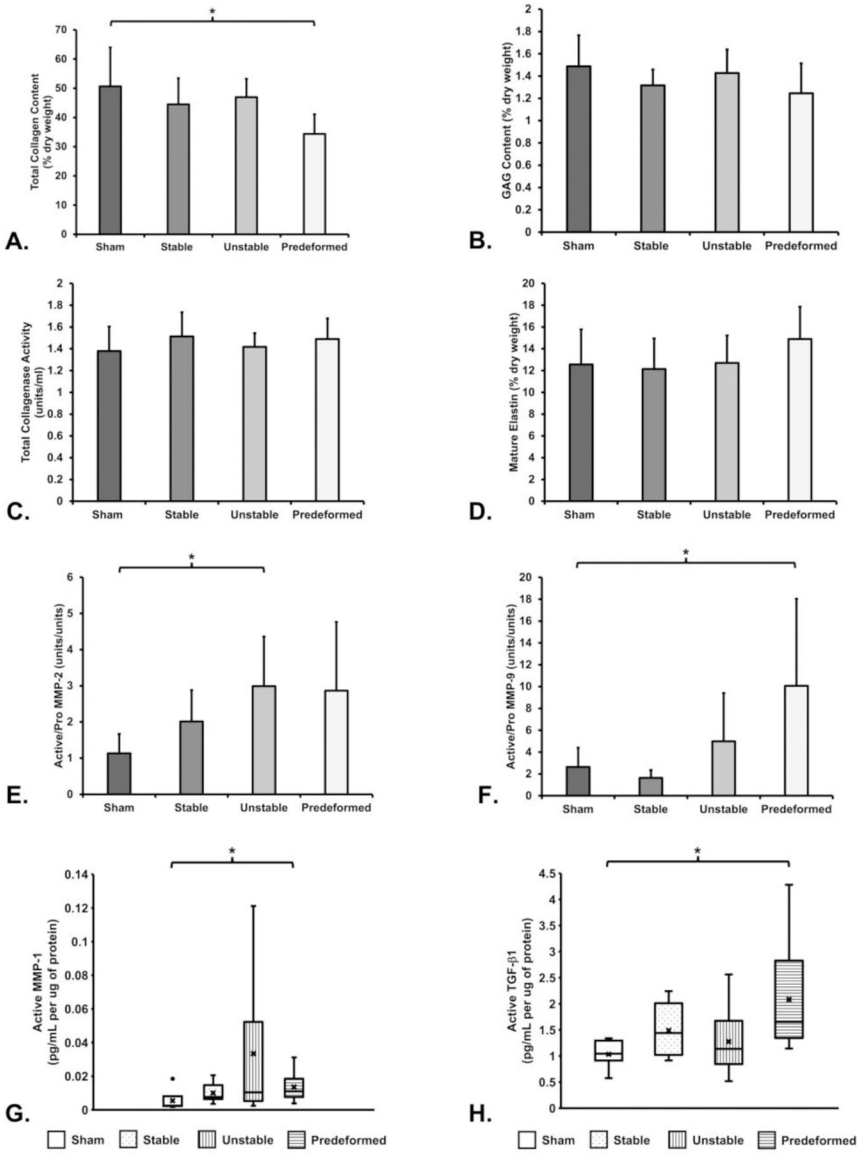

Figure 6: Biochemical analysis of the structural components of the vagina.
Significant differences from Sham indicated by (*).

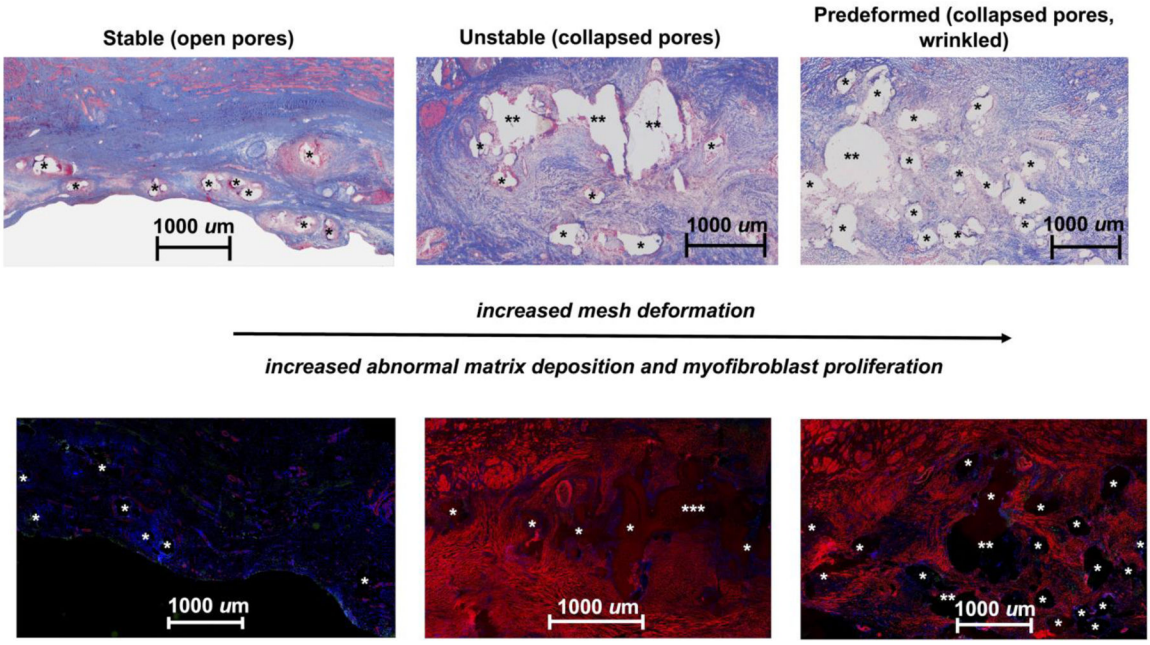

Figure 7: Abnormal matrix deposition and myofibroblast proliferation is increased with increasing mesh deformation.

Thin sections (7 μm) labeled with α-smooth muscle actin (red), apoptotic cells (green), and DAPI (blue) reveal normal matrix deposition (top left) and a very limited number of myofibroblasts (bottom left) in the open-pore Stable configuration. However, abnormal matrix deposition, as depicted by the faint pink staining surrounding mesh fibers (top middle and right images), which corresponds to myofibroblast, is observed in the Unstable (bottom middle) and Predeformed (bottom right) configurations. The small amount of red staining in the Stable group corresponds to the smooth muscle in blood vessels. Mesh fibers are delineated by asterisks (*), with more than one asterisk (** or ***) indicating more than one mesh fiber. The widely spaced fibers of the Stable group, corresponding to open pores, contrasts with the fiber crowding due to mesh deformation in the remaining two groups.

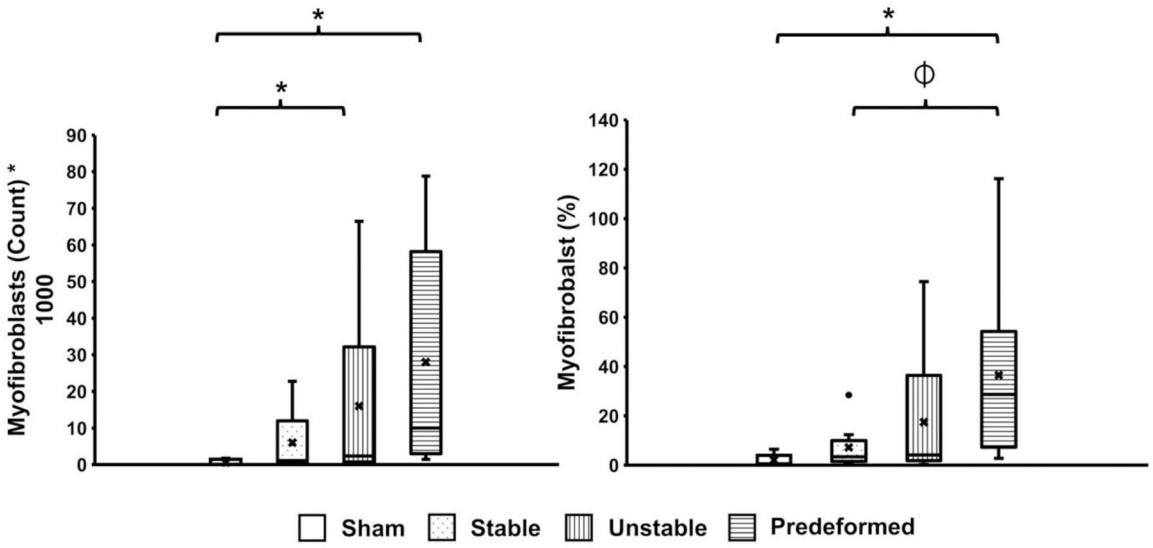

Figure 8: Number and percentage of myofibroblasts in the adventitia.

The percentage of myofibroblasts was obtained by normalizing the total number of myofibroblasts by the total number of cells. A significant difference in the percentage of myofibroblasts from Sham is indicated by *, and a significant difference in the percentage of myofibroblasts compared to Predeformed is indicated by Φ.

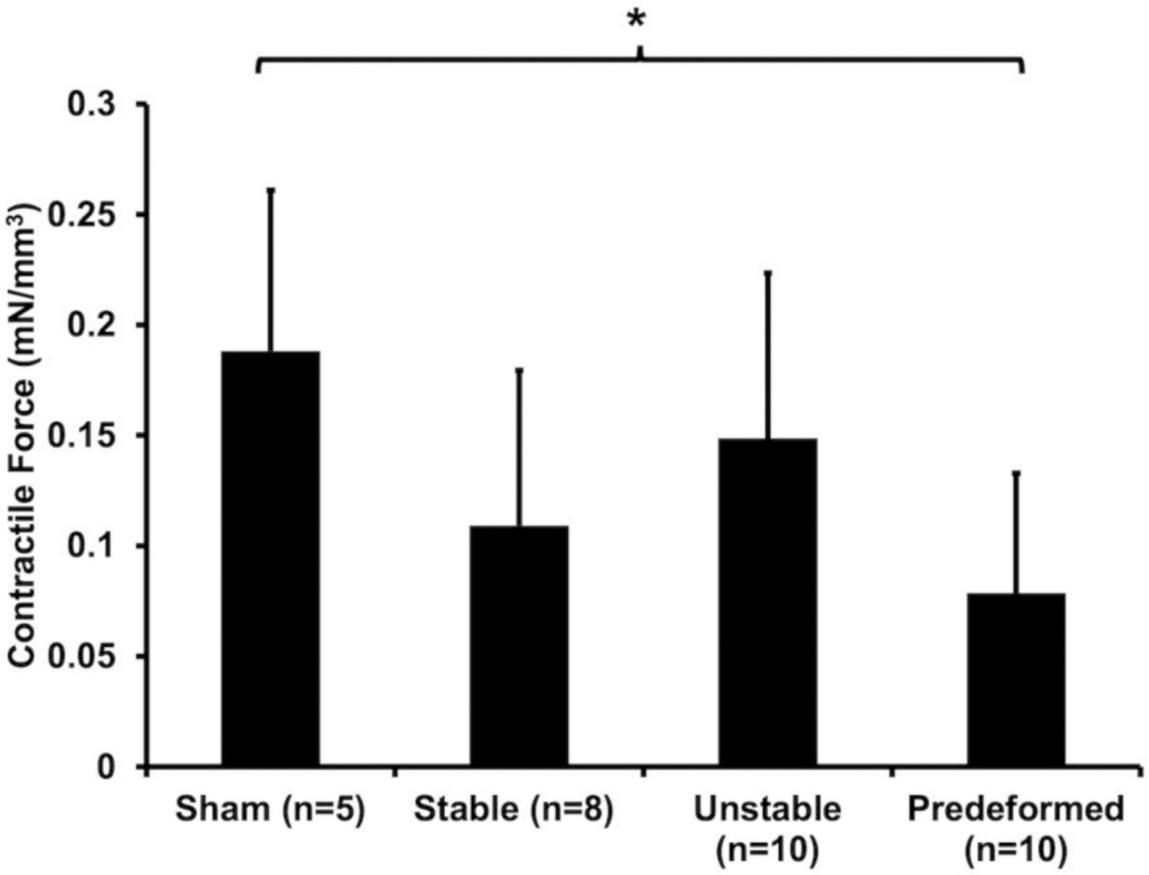

Figure 9: The contractile force, or force per volume (mN/mm^3) of the vagina following stimulation with 120 mM KCl.

A significant difference from Sham is indicated by *.

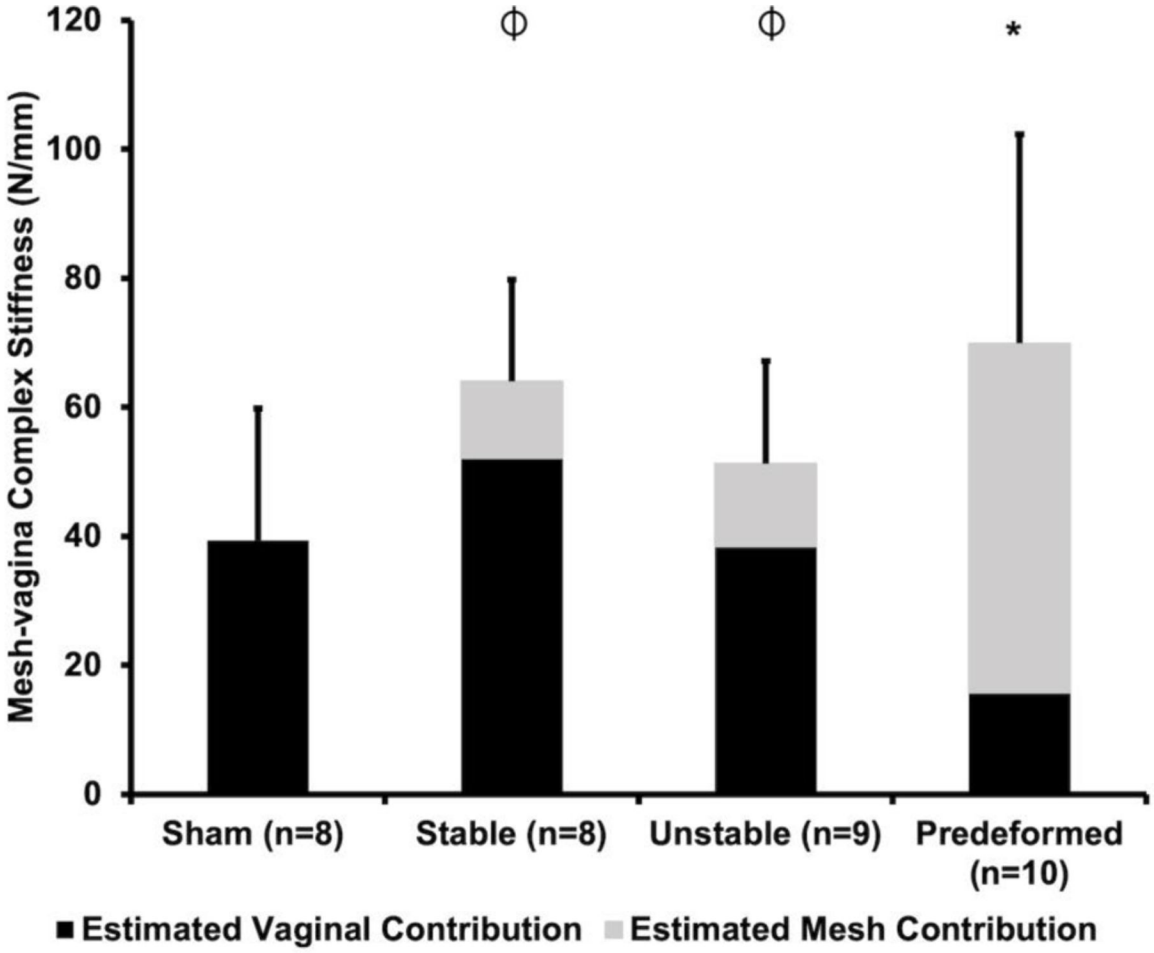

Figure 10: The stiffness (N/mm) of the mesh-vagina complexes (MVCs) obtained via ball-burst testing.

The estimated contributions of the vagina (black) and mesh (grey) to the overall MVC stiffness are delineated in black and grey, respectively. A significant difference in MVC stiffness from Sham is indicated by * and a significant difference in the estimated vaginal contribution compared to Predeformed is indicated by Φ.

Table 1:

Demographics of nonhuman primates.

	Age (yrs)	Weight (kg)	Gravidity	Parity
Sham (n=8)	9 ± 2	8.0 ± 1.8	2 (2 – 5)	2 (1 – 4)
Stable (n=9)	13 ± 2	8.5 ± 1.9	5 (2 – 7)	3 (2 – 7)
Unstable (n=10)	11 ± 3	8.3 ± 2.4	2 (2 – 3)	2 (1 – 3)
Predeformed (n=10)	12 ± 3	8.7 ± 1.5	4 (3 – 4)	3 (3 – 4)
Overall p-value	0.044[a]	0.90[a]	0.23[b]	0.17[b]

*Data represented as mean ± standard deviation or median (interquartile range).

*P-value obtained using [a]one-way ANOVA. Post-hoc testing for age via a Dunnett t-test revealed that Stable animals were significantly older than Sham (p=0.016). No significant differences were observed for Unstable (p=0.271) and Predeformed (p=0.099) animals relative to Sham.

*P-value obtained using [b]Kruskal-Wallis test.

Table 2:

Area of the subepithelium, muscularis, and adventitia normalized to the area of the vagina.

	Subepithelium (%)	Muscularis (%)	Adventitia (%)
Sham (n=7)	19 ± 10	55 ± 11	26 ± 13
Stable (n=8)	16 ± 10	51 ± 10	33 ± 13
Unstable (n=8)	16 ± 4	40 ± 11	44 ± 11
Predeformed (n=9)	15 ± 4	42 ± 10	45 ± 17
Overall p-value	0.78[a]	0.024[a]	0.045[c]
Sham vs Stable	0.79[b]	0.72[b]	0.28[d]
Sham vs Unstable	0.78[b]	0.024[b]	0.021[d]
Sham vs Predeformed	0.62[b]	0.042[b]	0.031[d]

* Data represented as mean ± standard deviation or median (interquartile range).

* P-value obtained using [a]one-way ANOVA followed by [b]Dunnett t-test.

* P-value obtained using the [c]Kruskal-Wallis followed by [d]Mann-Whitney test with a Bonferroni Correction ($p<0.016$ for significance).

* Note the area of the vagina did not include the area of the epithelium, given the high turnover of the epithelium.

Table 3:

Percentage of apoptotic cells within the respective layers of the vagina

	Subepithelium (%)	Muscularis (%)	Adventitia (%)
Sham (n=7)	0.05 (0.03 – 0.2)	0.01 (0.00 – 0.03)	0.3 (0.04 – 0.6)
Stable (n=8)	0.04 (0.01 – 0.1)	0.04 (0.01 – 0.06)	1.0 (0.7 – 5.4)
Unstable (n=6)	0.04 (0.01 – 0.1)	0.02 (0.01 – 0.05)	0.7 (0.6 – 1.4)
Predeformed (n=8)	0.5 (0.07 – 1.5)	0.2 (0.04 – 0.3)	1.3 (0.6 – 2.6)
Overall p-value	0.10[a]	0.025[a]	0.029[a]
Sham vs Stable	N/A	0.072[b]	0.009[b]
Sham vs Unstable	N/A	0.45[b]	0.073[b]
Sham vs Predeformed	N/A	0.009[b]	0.021[b]

* Data represented as mean ± standard deviation or median (interquartile range).

* P-value obtained using [a]Kruskal-Wallis Test followed by [b]Mann-Whitney test with a Bonferroni Correction ($p<0.016$ for significance).

* Note the amount of apoptosis was not quantified within the epithelium due to the high turnover of this layer.